



Deposited via The University of Leeds.

White Rose Research Online URL for this paper:

<https://eprints.whiterose.ac.uk/id/eprint/164711/>

Version: Accepted Version

Article:

Dunham, CK, O'Donnell, JP, Stuart, GW et al. (2020) A joint inversion of receiver function and Rayleigh wave phase velocity dispersion data to estimate crustal structure in West Antarctica. *Geophysical Journal International*. ggaa398. ISSN: 0956-540X

<https://doi.org/10.1093/gji/ggaa398>

© 2020, Oxford University Press. This is an author produced version of an article published in *Geophysical Journal International*. Uploaded in accordance with the publisher's self-archiving policy.

Reuse

Items deposited in White Rose Research Online are protected by copyright, with all rights reserved unless indicated otherwise. They may be downloaded and/or printed for private study, or other acts as permitted by national copyright laws. The publisher or other rights holders may allow further reproduction and re-use of the full text version. This is indicated by the licence information on the White Rose Research Online record for the item.

Takedown

If you consider content in White Rose Research Online to be in breach of UK law, please notify us by emailing eprints@whiterose.ac.uk including the URL of the record and the reason for the withdrawal request.

A joint inversion of receiver function and Rayleigh wave phase velocity dispersion data to estimate crustal structure in West Antarctica

C. K. Dunham¹, J. P. O'Donnell¹, G. W. Stuart¹, A. M. Brisbane²,
S. Rost¹, T. A. Jordan², A. A. Nyblade³, D. A. Wiens⁴, R. C. Aster⁵

August 19, 2020

(1) School of Earth and Environment, The University of Leeds, Leeds, LS2 9JT, UK

(2) British Antarctic Survey, National Environment Research Council, Cambridge, CB3 0ET, UK

(3) Department of Geosciences, The Pennsylvania State University, University Park, PA 16802, USA

(4) Department of Earth and Planetary Sciences, Washington University, St. Louis, MO 63160, USA

(5) Department of Geosciences, Colorado State University, Fort Collins, CO 80523, USA

Corresponding author: Charles Kingsley Dunham, email: c.k.dunham@leeds.ac.uk

Abbreviated title: Crustal structure of West Antarctica

1 **Abstract**

2 We determine crustal shear-wave velocity structure and crustal thickness at recently deployed seismic stations
3 across West Antarctica, using a joint inversion of receiver functions and fundamental mode Rayleigh wave
4 phase velocity dispersion. The stations are from both the UK Antarctic Network (UKANET) and Polar Earth
5 Observing Network/Antarctic Network (POLENET/ANET). The former include, for the first time, 4 stations
6 along the spine of the Antarctic Peninsula, 3 in the Ellsworth Land and 5 stations in the vicinity of the Pine
7 Island Rift. Within the West Antarctic Rift System (WARS) we model a crustal thickness range of 18-28 km,
8 and show that the thinnest crust (~ 18 km) is in the vicinity of the Byrd Subglacial Basin and Bentley Subglacial
9 Trench. In these regions we also find the highest ratio of fast ($V_s = 4.0-4.3$ km/s) (likely mafic) lower crust to
10 felsic/intermediate upper crust. The thickest mafic lower crust we model is in Ellsworth Land, a critical area
11 for constraining the eastern limits of the WARS. Although we find thinner crust in this region (~ 30 km) than in
12 the neighbouring Antarctic Peninsula and Haag-Ellsworth Whitmore block (HEW), the Ellsworth Land crust
13 has not undergone as much extension as the central WARS. This suggests that the WARS does not link with
14 the Weddell Sea Rift System through Ellsworth Land, and instead has progressed during its formation towards
15 the Bellingshausen and Amundsen Sea Embayments. We also find that the thin WARS crust extends towards
16 the Pine Island Rift, suggesting that the boundary between the WARS and the Thurston Island block lies in
17 this region, ~ 200 km north of its previously accepted position. The thickest crust (38-40 km) we model in this
18 study is in the Ellsworth Mountain section of the HEW block. We find thinner crust (30-33 km) in the Whitmore
19 Mountains and Haag Nunatak sectors of the HEW, consistent with the composite nature of the block. In the
20 Antarctic Peninsula we find a crustal thickness range of 30-38 km and a likely dominantly felsic/intermediate
21 crustal composition. By forward modelling high frequency receiver functions we also assess if any thick, low
22 velocity subglacial sediment accumulations are present, and find a 0.1-0.8 km thick layer at 10 stations within
23 the WARS, Thurston Island and Ellsworth Land. We suggest that these units of subglacial sediment could
24 provide a source region for the soft basal till layers found beneath numerous outlet glaciers, and may act to
25 accelerate ice flow.

26 **Keywords**

27 Antarctica

28 Joint inversion

29 Crustal structure

30 1 Introduction

31 West Antarctica has an enigmatic tectonic history, and is host to one of the largest continental rift systems
32 on Earth - The West Antarctic Rift System (WARS) (Dalziel and Elliot, 1982). The size and total amount
33 of extension encompassed by the WARS is still unclear due to the overlying West Antarctic Ice Sheet; this
34 uncertainty has implications for accurately achieving global plate circuit closure in tectonic reconstructions.
35 The WARS features deep bedrock elevations (Fretwell et al., 2013) and thin crust (Chaput et al., 2014), formed
36 as a result of late Mesozoic and Cenozoic extension between East and West Antarctica (e.g. Fitzgerald, 2002,
37 and references therein). The possible eastern progression of the WARS through Ellsworth Land is seismically
38 poorly constrained; studies suggest that it variably extends into both the Bellingshausen and Amundsen Sea
39 embayments (e.g. Gohl et al., 2015; Kalberg et al., 2015) and as far as the George VI Sound (Eagles et al.,
40 2009). It is also unclear if there is a linkage between the WARS and the neighbouring Weddell Sea Rift System,
41 a broad extensional province spanning the boundary between East and West Antarctica (Jordan et al., 2017).
42 In addition to the WARS, West Antarctica is comprised of a mosaic of antecedent crustal blocks separated
43 by the rift system, each with a distinct tectonic history. These are the Antarctic Peninsula, Thurston Island,
44 Haag-Ellsworth Whitmore (HEW) and Marie Byrd Land blocks (Fig. 1).

45 In this study we use a joint inversion of receiver function and Rayleigh wave phase velocity dispersion data
46 from UKANET and POLENET/ANET seismic stations across West Antarctica. The UKANET deployment
47 includes stations in the southern Antarctic Peninsula and Ellsworth Land for the first time. These stations
48 will provide valuable insight into the eastern termination of the WARS, and whether there is a connection
49 between the WARS and the Weddell Sea Rift System. Additionally we include stations from the UKANET -
50 POLENET/ANET Mini Array traverse which straddle the Thurston Island-WARS boundary, which will allow
51 for a better delineation of the northern edge of the WARS and its progression towards the Amundsen Sea
52 Embayment. By recovering a shear wave velocity-depth profile at each station we aim to constrain both crustal
53 thickness as well as the relative proportions of likely felsic/intermediate to mafic crust. We consider the crustal
54 structure we model at each station relative to its respective crustal block, then evaluate the overall tectonic
55 framework with regards to global analogues.

56 Another feature we aim to model is the presence of low seismic velocity subglacial sediment accumulations
57 beneath the West Antarctic Ice Sheet. The basal environment of the ice sheet plays a key role in its future
58 stability; two important controls on ice sheet models are basal heat flow and friction. Sediment accumulations
59 can provide a source region for basal till generation, which in turn has been proposed to be necessary for
60 the initiation of fast ice flow (Blankenship et al., 2001). As such, the location of thick subglacial sediment

61 accumulation can give an indication of likely or unlikely areas of fast ice flow. Subglacial sediment has been
62 inferred beneath sections of the West Antarctic Ice Sheet by previous receiver function studies (Winberry and
63 Anandkrishnan, 2004; Chaput et al., 2014), with estimates of sediment thickness up to 0.6 km in the Bentley
64 Subglacial Trench and 0.3 km in the Byrd Subglacial Basin. With the recently collected data used in this study
65 we aim to determine the distribution of major subglacial sediment accumulations across West Antarctica.

66 **2 Tectonic Setting**

67 Antarctica can be broadly divided into two tectonic domains divided by the Transantarctic Mountains (TAM).
68 East Antarctica features a thick Archean-Proterozoic cratonic crust, whilst West Antarctica consists of a mosaic
69 of crustal blocks with a varied history (e.g. Dalziel, 1992). The Antarctic Peninsula, Thurston Island and
70 Marie-Byrd Land are Paleozoic - Mesozoic accreted terranes which formed along the paleo-Pacific Gondwanan
71 margin, abutting East Antarctica (Dalziel and Elliot, 1982). The Jurassic breakup of Gondwana led to the
72 development of the Weddell Sea Rift System (e.g. Jordan et al., 2017), and subsequent Cretaceous-to-Cenozoic
73 extension between East Antarctica and Marie Byrd Land produced the WARS. In addition the HEW block,
74 which is considered a composite fragment of cratonic Gondwanan crust, was translated and rotated into its
75 current position following the break up of Gondwana.

76 **2.1 Haag-Ellsworth Whitmore block**

77 The HEW is a composite block consisting of the Haag-Nunataks, Ellsworth Mountains and Whitmore Moun-
78 tains. The block features atypical stratigraphy and crustal structure with respect to its surroundings, and is
79 proposed to be a remnant of Gondwanan lithosphere. The northwest-southeast structural trend within the HEW
80 is perpendicular to the neighbouring Thiel Mountains, which are part of the TAM (Storey and Dalziel, 1987),
81 suggesting that it has undergone significant rotation (Dalziel and Elliot, 1982). The HEW predominantly con-
82 sists of clastic metasedimentary rock with isolated igneous intrusions. Models of how the HEW arrived at
83 its current position are contentious. Paleomagnetic and geological interpretations (Schopf, 1969; Randall and
84 Mac Niocaill, 2004) include a 90° anticlockwise rotation and ~1500 km of translation from a pre-rift position
85 between South Africa and East Antarctica. A more recent geophysical study of the Weddell Sea by Jordan et al.
86 (2017) proposes a ‘less travelled’ model, whereby the HEW was originally located in the Weddell Sea region
87 before Jurassic extension. The model of Jordan et al. (2017) only accounts for a ~30° rotation, but they suggest
88 that deformation associated with the Permian Gondwanide Orogen may have provided the additional rotation
89 required to reconcile with previous observations.

90 **2.2 Antarctic Peninsula and Thurston Island**

91 The Antarctic Peninsula and Thurston Island evolved via sustained back arc magmatism and accretion due to the
92 subduction of the Phoenix plate beneath the Antarctic plate, before experiencing Cenozoic and Mesozoic uplift
93 (Birkenmajer et al., 1986; Grunow et al., 1991; Machado et al., 2005). To restore the Antarctic Peninsula to its
94 pre-Gondwanan break up position it must be rotated anticlockwise with respect to East Antarctica, eventually
95 aligning with the southern tip of South America (Fitzgerald, 2002). Modelling of radiogenic heat flux suggests
96 that the more silicic south and east of the Antarctic Peninsula have a higher heat flux ($\sim 81 \text{ mW m}^{-2}$) than the
97 north and west ($\sim 67 \text{ mW m}^{-2}$) (Burton-Johnson et al., 2017).

98 **2.3 West Antarctic Rift System (WARS)**

99 The WARS is an asymmetric rift system 750-1000 km in width and 3000 km in length (Behrendt et al., 1991).
100 The WARS developed as a consequence of predominately Cretaceous extension as the Antarctic Peninsula,
101 Thurston Island and Marie Byrd Land moved away from East Antarctica. It has been proposed that extension
102 occurred in two pulses; the major phase being a well documented period of broad extension across the whole
103 WARS in the Jurassic-Cretaceous (Luyendyk, 1995; Siddoway et al., 2004). A second pulse of extension
104 in the Neogene has been inferred in the sedimentary basins of the Ross Sea (e.g. Behrendt, 1999; Wilson
105 and Luyendyk, 2006), although to what extent the entire WARS was impacted is unclear. Although Neogene
106 extension appears to be preferentially concentrated along the East-West Antarctic boundary (e.g. Harry et al.,
107 2018), some geophysical studies have inferred concurrent extension in central and eastern portions of the WARS
108 (e.g. Damiani et al., 2014; Jordan et al., 2010; Winberry and Anandakrishnan, 2004). Lloyd et al. (2015) also
109 interpreted reduced seismic wavespeeds in the uppermost mantle beneath the WARS as the remnant thermal
110 signal of localised Neogene rifting. It has been proposed that WARS extension slowed at ca. 17 Ma (Granot
111 et al., 2013). The lack of recent significant seismicity in the region (e.g. Reading, 2007) combined with the very
112 low rates of tectonic intra-plate deformation (Donnellan and Luyendyk, 2004; Barletta et al., 2018), suggest that
113 the WARS is currently nearly inactive.

114 Given the ambiguity over the timing of extension and the substantial ice cover, estimates of total extension
115 encompassed by the WARS are poorly constrained. In the Ross Sea one-layer crustal stretching models assum-
116 ing a ~ 35 km initial thickness compared to the presently estimated 17-27 km thick crust suggest ~ 400 km of
117 extension (e.g. Behrendt and Cooper, 1991), whilst paleomagnetic modelling (DiVenere et al., 1994) indicates
118 a range from 440-1820 km. Paleomagnetic studies in this region are hampered by uncertainties in the amount
119 of rotation between West Antarctica's crustal blocks, and a lack of Cretaceous correlative poles. Improving
120 estimates of crustal thickness within the WARS will allow for more accurate modelling of the total extension.

121 **2.4 Recent geophysical investigation of crustal structure in West Antarctica**

122 Thanks to the gradual improvement in data coverage over the past 20 years, gravity studies have provided
123 valuable insight into Antarctica's tectonic structure (e.g. von Frese et al., 1999; Llubes et al., 2003; Block et al.,
124 2009; Jordan et al., 2010; O'Donnell and Nyblade, 2014). By inverting GRACE satellite gravity data Block
125 et al. (2009) modelled crust up to 46 km thick in East Antarctica and ~ 30 km in the centre of the WARS.
126 O'Donnell and Nyblade (2014) followed this study using an inversion of GOCO03S satellite gravity data,
127 finding a mean crustal thickness of 40 km in East Antarctica, and 24 km in West Antarctica. Aerogravity has
128 been used in more localised studies to image shorter wavelength structure. Jordan et al. (2010) focused on the
129 Pine Island Glacier region and model crust as thin as 19 km, suggesting that the region has been subject to
130 enhanced crustal thinning.

131 Since the deployment of POLENET/ANET, a number of studies have used the network to investigate crustal
132 structure across West Antarctica. Chaput et al. (2014) produced P-wave receiver functions from the POLENET/ANET
133 deployment and inverted them for crustal structure using a Markov Chain Monte Carlo approach. They found
134 20-25 km thick crust in the central WARS, surrounded by thicker adjacent crustal blocks: ~ 35 km in the HEW
135 block, ~ 30 km in Marie Byrd Land, and up to 45 km in the TAM. Additionally Chaput et al. (2014) inferred
136 a layer of low velocity subglacial sediment at many stations, with a thickness of up to ~ 0.4 km within the
137 Bentley Subglacial Trench. The presence of subglacial sediment in the region had previously been suggested
138 by Anandakrishnan and Winberry (2004), who inferred a ~ 0.6 km thick layer in the vicinity of the Bentley
139 Subglacial Trench.

140 To avoid the complex near surface reverberation present in P-wave receiver functions for stations on thick
141 ice sheets, Ramirez et al. (2016) used S-to-P receiver functions at POLENET/ANET stations across West
142 Antarctica. They found crustal thickness to be in general agreement with Chaput et al. (2014), varying from
143 19-29 km across the WARS. Ramirez et al. (2017) built upon this study by using a joint inversion of Rayleigh
144 wave phase velocities and P-wave receiver functions to image crustal structure at bedrock stations in West
145 Antarctica. They reported average crustal thicknesses of ~ 37 km in the HEW, ~ 30 km in Marie Byrd Land, 35
146 km at station MECK in the southern Antarctic Peninsula, and 38 km at THUR on the Thurston Island block.
147 Crustal thickness from Ramirez et al. (2017) generally agree with Chaput et al. (2014), however they estimated
148 the crust to be ~ 10 km thicker at stations MECK and THUR, which they attributed to the presence of a 10-20
149 km thick mafic lower crust.

150 Shen et al. (2018) combined fundamental mode Rayleigh wave phase and group velocity dispersion and
151 receiver functions in a Bayesian Monte Carlo algorithm to construct a 3-D shear velocity model of the crust and

152 uppermost mantle across Antarctica. In the WARS they find crustal thickness to range from 20-30 km, which is
153 consistent with aforementioned studies. Additionally Shen et al. (2018) image thinner crust and upper mantle
154 low velocity anomalies in the Amundsen Sea Embayment and Byrd Subglacial Basin, suggesting that these
155 regions have experienced recent extension. O'Donnell et al. (2019a) and O'Donnell et al. (2019b) modelled
156 fundamental mode Rayleigh wave phase velocities at periods 7-143 s across West Antarctica using seismic
157 ambient noise and earthquake data recorded on the UKANET and POLENET/ANET stations. O'Donnell et al.
158 (2019a) find ~ 22 km thick extended crust in the Ross and Amundsen Sea Embayments, and suggest that the
159 Cenozoic evolution of the WARS shows along strike variability. In addition O'Donnell et al. (2019a) model
160 crust to be ~ 32 -35 km thick in the southern Antarctic Peninsula and ~ 30 -40 km thick in the HEW.

161 **3 Data and Methods**

162 **3.1 Stations**

163 The data used in this study were recorded on 33 stations (see Supplementary Table 1) distributed across the
164 eastern WARS, Thurston Island, HEW and southern Antarctic Peninsula from the UKANET (2016-2018) and
165 POLENET/ANET (2008-) seismic networks (Fig. 1). The stations are situated on ice as well as on bedrock,
166 with rock sites typically on the flanks of nunataks. POLENET/ANET consists of long term backbone stations
167 distributed across West Antarctica, which feature a mixture of cold-rated Guralp CMG-3T 120 s and Nanomet-
168 rics Trillium 240 s sensors, sampling at 1 and 40 samples per second (sps). The UKANET (2016-2018) and
169 POLENET-ANET mini-array (2015-2017) were denser but shorter term deployments, with the former featuring
170 Guralp CMG-3T 120 s seismometers which sampled at 1 and 100 sps, and the latter Nanometrics 120 s PH
171 sensors.

172 **3.2 Receiver functions**

173 P-wave receiver function analysis is a powerful tool for estimating depths to significant seismic impedance
174 contrasts beneath the receiver, and are produced at each station via a deconvolution of the vertical from the
175 radial component for teleseismic earthquakes (e.g. Langston, 1979). For receiver function analysis, we use
176 teleseismic earthquakes in the epicentral distance range of 30° to 90° with magnitude $M_w \geq 5.8$ from 2008-
177 2018. Prior to deconvolution we cut each seismogram from 10 s before to 120 s after the theoretical P-wave
178 arrival according to the IASP91 global model (Kennett and Engdahl, 1991), and then de-trend, taper and high
179 pass filter at 0.05 Hz. We rotate the east and north components of the seismogram to the great circle path to
180 produce radial and transverse components, then compute receiver functions using the Extended Multi-Taper
181 Receiver Function (ETMTRF) method of Helffrich (2006). ETMTRF has successfully been applied at noisy

182 stations, such as in ocean island studies (Lodge and Helffrich, 2009) where the noise conditions are similar to
183 the Antarctic Peninsula (Anthony et al., 2015).

184 We produce receiver functions at three maximum frequencies: 0.5 Hz, 2 Hz, and 4 Hz. The 0.5 Hz and 2 Hz
185 maximum frequency receiver functions are used in the joint inversion, whilst the 4 Hz receiver functions are
186 used in forward modelling for subglacial sediment. The 0.5 Hz maximum frequency receiver functions will im-
187 prove our observation of deeper structure, whilst the higher frequency receiver functions offer better resolution
188 of the near surface ice/sediment (e.g. Piana Agostinetti and Malinverno, 2018). Strong multiple reverberations
189 (Fig. 2) complicate the time series and arise when thin low velocity layers, such as ice and sediment, are present
190 beneath the seismic station. These ice/sediment reverberations can interfere with important crustal phases from
191 the Moho (e.g. P_{sMoho}). Fig. 2 shows 2 Hz receiver functions generated from 2016-18 at UKANET station
192 PIG1 binned by slowness and back azimuth. The early portion of the receiver function is influenced by the
193 P-wave reverberation in the ice/subglacial sediment layers, contaminating the expected arrival of crustal phases
194 e.g. P_{sMoho} . For a 30 km thick crust the P_{sMoho} phase would be expected to arrive at 3-4 s, whilst the often-
195 high amplitude reflected phases from the base of the ice sheet could arrive at roughly the same time depending
196 on ice thickness.

197 **3.3 Forward modelling to infer subglacial sediment**

198 We forward model high frequency receiver functions to detect if any subglacial sediment is present at each
199 station. Ice thickness is constrained to less than ± 100 m by BEDMAP2 (Fretwell et al., 2013) at most stations,
200 and is treated as a uniform layer in the forward modelling. Ice velocity is fixed at $V_p = 3.87$ km/s, $V_s = 1.9$ km/s
201 and density at $\rho = 0.9$ g/cm³ based on seismic studies of polar ice (Kohnen, 1974).

202 We use the grid search forward modelling approach of Anandakrishnan and Winberry (2004) to characterize
203 any potential subglacial sediment (Fig. 3). We allow subglacial sediment thickness to vary from 0-1 km, and
204 V_s from 0.2-2.0 km/s; V_p and ρ are calculated using the empirical relations defined by Brocher (2005). A
205 synthetic receiver function is generated, having been preprocessed and deconvolved with the same parameters
206 as the data at a maximum frequency of 4 Hz. To analyse model fit we compute the L_2 norm residual between
207 the synthetic and observed stacked 4 Hz receiver function over the first 4 s. By analysing misfit over the first 4
208 s we aim to exploit the shift in the relative timing of the ice conversions ($P_{s_{ice}}$) and reverberations ($P_p P_{s_{ice}}$)
209 introduced by the addition of a subglacial sediment layer.

210 To obtain 95% confidence intervals for the grid search result we use a bootstrap resampling scheme (Fig.
211 3c). We produce 5000 randomly sampled receiver function stacks from the data and then compute the misfit

212 with respect to the best fitting synthetic receiver function produced by the forward modelling. Assuming a
213 normal Gaussian distribution of misfit we then extract 95% confidence limits. Subglacial sediment thickness
214 is generally reasonably well constrained to within ± 0.2 km, whilst sediment V_s is less so, varying from ± 0.2
215 km/s to ± 1.0 km/s at different stations (see Supplementary Table 1).

216 **3.4 Joint inversion for crustal structure**

217 Given that receiver functions are a time series, conversion of a time interval to depth requires knowledge of the
218 corresponding velocity structure. Rayleigh wave phase velocity dispersion data is sensitive to average shear
219 wave velocity structure, therefore it is often advantageous to use a joint inversion of Rayleigh wave dispersion
220 curves and receiver functions when aiming to constrain crustal structure. To estimate crustal thickness and
221 obtain a crustal shear wave velocity model at each station, we use the method of Julia et al. (2000) for jointly
222 inverting receiver functions and Rayleigh wave phase velocity dispersion data. The method produces a lay-
223 ered shear velocity-depth profile by solving a linearised damped least-squares joint inversion. This inversion
224 technique also allows for the inclusion of *a priori* information on layer depths and velocities.

225 In the initial model at each station the crust is parameterised as 2.5 km thick layers with a gradually increasing
226 shear wave velocity from 3.4-4.0 km/s and an overall crustal thickness of 35 km. The crust overlies a uniform
227 upper mantle with a V_s of 4.5 km/s. At each station we include the best fitting near surface subglacial sediment
228 identified in the forward modelling, and ice thickness from BEDMAP2 (Fretwell et al., 2013). Including the
229 ice layer in the initial model allows the additional complexity in the receiver function to be accounted for in
230 the joint inversion process. A similar approach was taken by Shen et al. (2018), who find the incorporation of
231 receiver functions provides additional constraints on crustal structure than inverting surface wave data alone.
232 The subglacial sediment layer thickness is fixed, but V_s is allowed to change in the inversion process, as the
233 absolute shear wave velocity is loosely constrained in the forward modelling step. Layer thickness is fixed at
234 2.5 km from the base of the ice/sediment to 50 km, and at 5 km from 50 km to 80 km.

235 At each station we use a Rayleigh wave phase velocity dispersion curve in the 8-50 s period range modelled
236 in the O'Donnell et al. (2019a) and O'Donnell et al. (2019b) studies. The dispersion curves are constrained to
237 within ± 0.05 km/s at all periods. For more information on the generation of the Rayleigh wave phase velocity
238 dispersion curves and the associated uncertainty please see O'Donnell et al. (2019a) and O'Donnell et al.
239 (2019b). We then jointly invert this with receiver functions stacked into narrow ray parameter bins of 0.040-
240 0.049, 0.050-0.059, 0.060-0.069 and >0.070 s km⁻¹ at two maximum frequencies, 0.5 Hz and 2 Hz (Fig. 4).
241 As described in Julia et al. (2000) we equalize the number of data points and physical units in both data sets,
242 allowing us to give each equal weight in the joint inversion. The ± 0.05 km/s uncertainty in the Rayleigh wave

243 phase velocity dispersion data was included as part of the inversion process.

244 To evaluate uncertainty in the final V_s models arising from the stacked receiver functions, we use a boot-
245 strapping procedure which involves repeating the inversion process 500 times each with randomly resampled
246 receiver function stacks (e.g. Bao et al., 2015; Emry et al., 2015). Each bootstrap receiver function stack was
247 produced by randomly selecting receiver functions from the dataset with replacement and then stacking. To
248 determine the corresponding uncertainty for our crustal thickness value, we inspect the bootstrap shear wave
249 velocity limits of layers neighbouring the interpreted Moho from the full ensemble of bootstrap models. We
250 find that the error in our velocity models is constrained to ± 0.15 km/s and the Moho depth to ± 2.5 -5 km at
251 most stations. These uncertainty constraints are comparable to other studies of crustal thickness in the region
252 (e.g. Chaput et al., 2014; Ramirez et al., 2017). Additional uncertainty in the joint inversion results arises due to
253 the V_p/V_s ratio remaining fixed in the inversion. After testing the joint inversion with a range of crustal V_p/V_s
254 ratios (1.7-1.8), we find that the uncertainty arising from the V_p/V_s ratio is within the bootstrap error bounds,
255 and the interpreted Moho would remain the same (see supplementary material).

256 **3.5 Interpreting final shear wave velocity-depth models**

257 The output from the joint inversion is a shear velocity-depth profile (Fig. 4), which requires interpretation to
258 determine the crustal thickness at each station. We interpret the Moho in each final model to be the depth at
259 which there is a >0.25 km/s shear wave velocity increase in the 4.0-4.3 km/s range, or when the shear wave
260 velocity exceeds 4.3 km/s following Ramirez et al. (2017). As stated in Ramirez et al. (2017) lower crustal
261 shear wave velocities derived from V_p/V_s ratios from experimental data (e.g. Christensen and Mooney, 1995;
262 Christensen, 1996; Holbrook et al., 1992) rarely exceed 4.3 km/s. Shear wave velocities at or above 4.3 km/s
263 are therefore more likely to represent upper mantle than crustal lithologies. Whilst a shear wave velocity of 4.3
264 km/s is not globally characteristic of the upper mantle, the expectation of an instantaneous jump in V_s to values
265 exceeding 4.5 km/s as indicated by global velocity models may not always be reasonable. Lebedev et al. (2009)
266 suggest that upper mantle velocities increase with depth from the Moho to a maximum before decreasing again
267 due to the spinel peridotite-garnet peridotite transition. When interpreting the Moho we therefore seek a rapid
268 increase or jump in shear wave velocity from likely crustal values to values exceeding 4.3 km/s range, rather
269 than when 4.5 km/s is reached.

270 Our method for interpreting the Moho depth in the final shear wave velocity models follows other similar
271 studies of crustal thickness in the same region (O'Donnell et al., 2019a; Ramirez et al., 2017). Despite this,
272 a sharp jump from typical lower crustal to upper mantle shear wave velocities is not present at all stations.
273 This is likely due to the Ps_{Moho} phase being masked by the reverberations from shallow low velocity structure,

274 such as the ice layer, in the receiver function. Our modelled crustal thickness at stations where this is the case
275 are therefore predominantly controlled by the Rayleigh Wave dispersion data, and have a higher associated
276 uncertainty.

277 To further characterise the composition and nature of the crust at each station, we divide the crust into
278 likely sedimentary, felsic/intermediate upper crust, and mafic lower crustal layers based on the modelled shear
279 wave velocity structure. Studies of crustal structure and composition (e.g. Rudnick and Fountain, 1995) have
280 suggested that felsic-to-intermediate crust tends to have a shear wave velocity of <3.9 km/s, whilst common
281 lower crustal mafic lithologies tend to have shear wave velocity of >3.9 km/s. We suggest that crustal layers
282 with a $V_s < 3.2$ km/s likely represents sediments, V_s of 3.2-4.0 km/s represent likely felsic to intermediate
283 crust, whilst a V_s of 4.0-4.3 km/s indicate likely mafic lower crust.

284 **4 Results**

285 At each station we have produced models of crustal thickness and shear wave velocity structure (Fig. 5). The
286 Antarctic Peninsula and HEW blocks host the thickest crust we interpret in this study, with crustal thickness
287 ranges of 30-38 km and 30-40 km respectively. In both these blocks we also find the largest relative abundance
288 of likely felsic-to-intermediate crust with a V_s from 3.2-3.9 km/s. The thinnest crust we interpret is within
289 the WARS, with a thickness range of 18-28 km. Within the WARS we also model the overall highest relative
290 proportion of high velocity, likely mafic lower crust to likely felsic/intermediate crust (Fig. 5).

291 Within the HEW block we find the thickest crust at stations HOWD, WILS and UNGL, at 40, 38, and 38 ± 5
292 km respectively. All three stations are located within the Ellsworth Mountain section of the block, whilst
293 stations within the Whitmore Mountain and Haag Nunatak sections of the block feature a thinner crust at ~ 33
294 km. Given that most stations within the HEW and Antarctic Peninsula are situated on the flanks of nunataks
295 and on bedrock, no subglacial sediment was identified within these blocks.

296 Stations ELSW and KEAL are located close to the northern edge of the HEW block in Ellsworth Land, and
297 feature fundamentally different crust to that seen within the interior of the HEW. We observe a shallower Moho
298 at 30 ± 2.5 km with a seemingly two layer crust. A slow upper crust of ~ 3.4 km/s overlies a fast and relatively
299 uniform middle and lower crust with an average V_s of 4.0 km/s. The internal crustal structure at these stations
300 is similar to those in the centre of the WARS, however both feature a deeper Moho. Additionally we identify
301 subglacial sediment at both stations with a thickness of 0.1-0.2 km and V_s of ~ 1.0 km/s.

302 In the center of the WARS we find slow upper crustal layers $V_s < 3.2$ km/s, underlain by 10-15 km of likely
303 felsic crust and a 5-10 km thick likely mafic lower crust with a $V_s > 4.0$ km/s. The thinnest crust imaged in this
304 study at 18-20 km come from stations MA07, MA08 and UPTW, all of which lie in the vicinity of either the
305 Byrd Subglacial Basin or Bentley Subglacial Trench.

306 Subglacial low velocity sediment identified in the forward modelling is present at 10 stations within the
307 WARS and Thurston Island and Ellsworth Land with a range of thicknesses from 0.1-0.8 km. Shear wave
308 velocity in these layers varies from 0.4-1.6 km/s (see supplementary material). At stations MA09 and MA10
309 our best fitting model features a 0.1-0.3 km thick subglacial layer with a V_s of ~ 1.9 km/s which is close to that
310 of ice (Kohnen, 1974), indicating that at these stations there may be thicker ice than indicated by BEDMAP2.
311 At station UPTW we use the subglacial sediment thickness and V_s from Chaput et al. (2014) to parameterise
312 the initial model, as our forward modelling did not produce a stable solution at this station.

313 **5 Discussion**

314 To build on our current knowledge of West Antarctica's crustal framework, we consider our estimates of crustal
315 thickness and shear wave velocity structure in the context of the regional tectonics. Improving our grasp on
316 West Antarctica's tectonic framework is essential for building a comprehensive understanding of the region's
317 evolution. By inspecting the broad crustal structure of each crustal block, we can contrast West Antarctica's
318 tectonic mosaic with analogous regions worldwide.

319 Our crustal thickness estimates from West Antarctica are compatible with other seismic and gravity studies
320 conducted in the region, as summarised by Table 1. In the West Antarctic Rift System our crustal thickness
321 range of 18-28 km is in good agreement with seismic (Winberry and Anandkrishnan, 2004; Baranov and
322 Morelli, 2013; Chaput et al., 2014; Ramirez et al., 2016; Shen et al., 2018) and gravity derived crustal thickness
323 estimates (Jordan et al., 2010; O'Donnell and Nyblade, 2014). Stations BYRD, DNTW, UPTW and WAIS are
324 featured in previous receiver function (Chaput et al., 2014) and S-wave receiver function (Ramirez et al., 2016)
325 studies. Our crustal thickness estimates agree within uncertainty bounds with Chaput et al. (2014) at all four
326 stations, but we find 10 km thinner crust at UPTW than Ramirez et al. (2016).

327 **5.1 Tectonic interpretation of V_s profiles**

328 Fig. 6 shows our crustal thickness estimates plotted alongside the ambient seismic noise derived crustal thick-
329 ness model of O'Donnell et al. (2019a). Given the similar input dispersion datasets we see a good general
330 agreement between crustal thickness estimates (see Supplementary Table 1), however the inclusion of receiver

331 functions in this study improves resolution of crustal structure and discontinuities at each station. Our mini-
332 mum crustal thickness comes from the Byrd Subglacial Basin, and is ~ 5 km thinner than that of O'Donnell
333 et al. (2019a). Given that the spatial resolution of the ambient noise crustal model of O'Donnell et al. (2019a)
334 is on the order of ~ 300 km it is likely that these narrow rifts are not fully resolved. As such, the combination
335 of both the crustal thickness model of O'Donnell et al. (2019a) and the joint inversion results from this study
336 can provide an enhanced image of West Antarctica's crustal mosaic.

337 We find the thinnest crust in this study in the centre of the West Antarctic Rift System; an area which also
338 hosts the Byrd Subglacial Basin and Bentley Subglacial Trench. In addition in this area we find the highest pro-
339 portion of fast, likely mafic lower crust as shown by Fig. 5. The isostatic impact of the potentially high relative
340 abundance of dense mafic crust may be a contributing factor in the region's extremely low observed bedrock
341 elevation (Fretwell et al., 2013), in combination with the isostatic adjustment of the thick ice overburden. We
342 model a thinner crust and higher proportion of mafic lower crust in comparison to the Mesozoic/Cenozoic ex-
343 tensional type section of Rudnick and Fountain (1995); our WARS models are more in line with the active rifts
344 that Rudnick and Fountain (1995) analyse. We therefore suggest that the thin crust with a thick mafic lower
345 crustal layer we model in the vicinity of the Byrd Subglacial Basin and Bentley Subglacial Trench is supportive
346 of additional Neogene rifting impacting the central and eastern WARS (e.g. Jordan et al., 2010). A compara-
347 ble rift system to the WARS in terms of scale (but not elevation) is the Cenozoic Basin and Range province,
348 which features crust ranging from 30-35 km thick (Zandt et al., 1995). The thinner WARS crust supports the
349 suggestion that it has undergone enhanced localised thinning relative to the Basin and Range. The highly mafic
350 lower crust we model, in combination with the localised deep subglacial basins of the Byrd Subglacial Basin
351 and Bentley Subglacial Trench, is comparable to the southern section of the Kenya Rift Zone and Baikal Rift
352 Zone (Thybo and Artemieva, 2013). In these regions the presence of mafic underplating and sills in the lower
353 crust has lead to magma compensated crustal thinning, and a deep rift graben forming above.

354 Within the Antarctic Peninsula we find an average crustal thickness of 35 km with $\sim 75\%$ of the crust being
355 composed of lower velocity likely felsic to intermediate material (Fig. 5). As such, the crustal thickness and
356 velocity structure that we see in the Antarctic Peninsula is consistent with an arc tectonic environment (e.g.
357 Christensen and Mooney, 1995). Models of subglacial heat flux on the Antarctic Peninsula have suggested
358 that the southern and eastern sections of the Peninsula have a high flux, up to 100 mWm^{-2} in places (Burton-
359 Johnson et al., 2017). Areas of elevated heat flux on the Antarctic Peninsula coincide with UKANET stations
360 ATOL, BREN and WELC, all of which show relatively slow upper and mid crustal average shear wave veloc-
361 ities and a thin mafic lower crust with respect to the total crustal thickness (Fig. 5). A predominantly felsic to
362 intermediate crustal composition in this region would provide capacity for high radiogenic heat production as

363 suggested by Burton-Johnson et al. (2017).

364 We find along strike variability in crustal thickness within the HEW block, from the Haag Nunatak section
365 through the Ellsworth Mountains and into the Whitmore Mountains. We find the thickest crust in this study
366 in the Ellsworth Mountain section of the HEW block at 38-40 km at stations HOWD, UNGL and WILS.
367 Stations within the Whitmore Mountain section of the HEW block image a thinner (30-33 km), and more
368 felsic-like crust than the Ellsworth Mountain section of the block (Fig. 5). This spatial variability of crustal
369 thickness and structure within the HEW block has previously been noted by other seismic and aerogravity
370 studies (Jordan et al., 2010; Chaput et al., 2014; Heeszel et al., 2016; Ramirez et al., 2017; O'Donnell et al.,
371 2019a). The UKANET station FOWL is the first to be deployed in the Haag Nunatak section of the HEW block,
372 and here we infer ~ 7.5 km thinner crust (33 ± 2.5 km), and a contrasting crustal structure to the neighbouring
373 POLENET/ANET stations in the Ellsworth Mountains (HOWD, UNGL, WILS). The fast upper crust we infer
374 at FOWL may be indicative of additional potentially mafic intrusions in the upper crust relative to surrounding
375 stations in Ellsworth Land and the HEW. The basement exposure of the Haag Nunataks is among the oldest
376 sampled in West Antarctica at ~ 1 Ga (Millar and Pankhurst, 1987), and the crustal thickness we model is ~ 10
377 km thinner than the characteristic seismically imaged Proterozoic crust of Durrheim and Mooney (1991). The
378 Proterozoic crust studied in Durrheim and Mooney (1991) also includes a thick high velocity layer at the base
379 of the crust which is attributed to basaltic underplating, and at FOWL we infer a 7.5 km thick likely mafic
380 lower crust. A possible explanation for the reduced crustal thickness we model at FOWL relative to other
381 characteristic Proterozoic crust is through lower crustal flow into neighbouring tectonic blocks. Lower crustal
382 flow from the Haag Nunataks into the Weddell Sea Rift System in the Jurassic has previously been proposed
383 by Jordan et al. (2017), which would have acted to enhance Weddell Sea Rift System extension.

384 **5.2 Refining the bounds of the West Antarctic Rift System**

385 According to the crustal block boundaries of Dalziel and Elliot (1982), the tectonic block in which UKANET
386 stations ELSW and KEAL are situated is indeterminate. This region is crucial for revealing any possible
387 connectivity with the Weddell Sea Rift System. The overall crustal thickness at the Ellsworth Land stations
388 (30 ± 5 km) is comparable to the neighbouring Haag Nunataks, yet the internal crustal structure features a
389 thicker (10-20 km thick) high-velocity likely mafic lower crust. As previously noted, the potential abundance
390 of dense mafic lower crust may be responsible for the deep bedrock elevations in the region, whilst the overall
391 thicker crust suggests that Ellsworth Land has undergone less extension than the central WARS. The presence
392 of extensive mafic underplating in the neighbouring Weddell Sea Rift System has been attributed to plume
393 related Jurassic magmatism by Jordan et al. (2017); a similar mechanism may have been responsible for the

394 thick mafic lower crust which we model in Ellsworth Land. An alternative interpretation is that lower crustal
395 flow from the Haag Nunataks transferred mafic material not only to the Weddell Sea Rift System but also
396 into Ellsworth Land. Were this to be the case then a lateral pressure gradient in the lower crust would have
397 to have been present to facilitate upper crustal extension, suggesting that the region has been subject to some
398 stretching. The disparity in both crustal thickness and structure with regards to the central WARS suggests that
399 the rift system did not substantially propagate into Ellsworth Land. We therefore suggest that there is not a
400 direct linkage between the WARS and Weddell Sea Rift System, and that the WARS instead propagated in the
401 direction of the Bellingshausen and Amundsen Sea embayments.

402 The UKANET - POLENET Mini Array traverse (PIG1 - MA06) crosses from Thurston Island into the West
403 Antarctic Rift System, and as such can be utilised to better constrain the northern boundary of the WARS. Fig.
404 7 shows the shear wave velocity-depth profiles from the Pine Island Glacier station traverse. At stations in the
405 centre of the West Antarctic Rift System (PIG3 - MA05) we find crust with a consistent thickness of 23-25 km,
406 whilst at Thurston Island stations (THUR - PIG2) we find a thicker crust of 28-30 km. Our findings therefore
407 support the suggestion that the WARS - Thurston Island block boundary lies in the vicinity of the Pine Island
408 Rift. A number of previous studies have proposed that the Pine Island Rift is a branch of the WARS (Damiani
409 et al., 2014; Gohl et al., 2007; Gohl, 2012; Jordan et al., 2010), and that the region between the Pine Island
410 Rift and the Byrd Subglacial Basin is a transitional crustal boundary zone (Diehl, 2008). The gradual decrease
411 in crustal thickness that we model from PIG2 to MA01 is supportive of this region being a transitional area
412 from Thurston Island to WARS crust. The transition from WARS to Thurston Island crust is more subtle than
413 on the opposing flank of the rift system. The sharp change in crustal character and bedrock elevation between
414 the WARS and HEW block suggests that this boundary may instead be more fault controlled than the Thurston
415 Island-WARS flank.

416 Gohl (2012) and Bingham et al. (2012) both suggest that major ice streams in West Antarctica exploit tectonic
417 lineaments created by rifting. Our estimates of crustal thickness support the suggestion that Pine Island Glacier
418 could be steered by WARS rift structures. Were the Thurston Island-WARS boundary to be in the vicinity of
419 the Pine Island Rift then that would imply a ~ 200 km shift from its previously accepted position in Dalziel
420 and Elliot (1982). If the WARS is indeed 200 km wider, then there are implications for modelling plate circuit
421 closure and for the total amount of extension encompassed by the WARS. The new boundary we propose also
422 suggests that the WARS extends further towards both the Amundsen Sea and Bellingshausen Sea embayments
423 than previously thought (Fig. 6).

424 **5.3 Estimating subglacial sediment thickness**

425 Fig. 6 features a map of all stations at which we identify low velocity subglacial layers in the forward mod-
426 elling. Subglacial layers of this thickness (0.1-0.8 km) and shear wave velocity (0.4-1.6 km/s) are indicative of
427 unlithified, soft and possibly saturated sediment (Winberry and Anandakrishnan, 2004). We find low velocity
428 subglacial layers at 10 stations within the WARS, Thurston Island and Ellsworth Land, with the majority at sta-
429 tions in the vicinity of the Byrd Subglacial Basin and Bentley Subglacial Trench. These deep subglacial basins
430 could provide ample accommodation space for the accumulation of relatively thick subglacial sediment, which
431 in turn may have provided the basal till to accelerate regional ice flow. The abundance of soft unlithified sedi-
432 ment in the central portion of the WARS could well have been a contributing factor for the fast flow observed
433 in the Thwaites Glacier region (Rignot et al., 2011). Soft deforming till layers have been identified in the upper
434 reaches of Thwaites Glacier using seismic reflection (Muto et al., 2019), much of which may have been sourced
435 from the thick subglacial sediment accumulations we model in the Byrd Subglacial Basin. Subglacial sediment
436 has also been identified within the deep basins of the central WARS by Pourpoint et al. (2019), who used a
437 joint inversion of receiver functions, Rayleigh and Love dispersion, and Rayleigh wave horizontal-to-vertical
438 amplitude ratio. Pourpoint et al. (2019) modelled sediment to be 1.5 km thick beneath station MA08, and >0.5
439 km thick at stations DNTW, UPTW, MA06 and MA07.

440 In addition we find 0.1-0.2 km thick subglacial sediment present in the vicinity of Pine Island Glacier at PIG2
441 and PIG4, another region of fast ice flow. Large-scale sedimentary deposits have previously been identified
442 using seismic reflection (Brisbourne et al., 2017), and aerogravity models indicate there could be ~ 0.8 km
443 thick sediments near the glacier's grounding line (Muto et al., 2016).

444 Another region in which we infer the presence of low velocity subglacial sediment is at stations ELSW and
445 KEAL (Fig. 6), both of which lie upstream of the Rutford Ice Stream and Evans Ice Stream. The Rutford Ice
446 Stream flows at a velocity up to ~ 400 m a⁻¹ (Gudmundsson, 2006), yet it has a gentle surface slope relative
447 to other fast flowing West Antarctic ice streams suggesting that the basal driving stress is low (e.g. MacAyeal
448 et al., 1995). To accommodate such a high velocity with a low basal driving stress the basal friction must also
449 be low, implying that soft sediment must be present. A number of studies have confirmed the presence of large
450 scale sedimentary bedforms beneath the Rutford Ice Stream, using both seismic surveying and ice penetrating
451 radar (King et al., 2007; Smith and Murray, 2009). In the Evans Ice Stream, Vaughan et al. (2003) measured
452 acoustic impedance to reveal that the entire bed of the ice stream consists of dilated sediment. The 0.1-0.3
453 km thick low velocity sedimentary layer that we model at ELSW and KEAL could have provided an upstream
454 source for the subglacial sediments identified beneath the Rutford Ice Stream and Evans Ice Stream, which has
455 subsequently acted to accelerate flow.

456 **6 Conclusions**

457 Through a joint inversion of receiver functions and Rayleigh wave phase velocity dispersion data, we image
458 crustal shear velocity structure at 33 seismic stations across West Antarctica. The thinnest surveyed crust in
459 our study lies within the West Antarctic Rift System (18-28 km), bounded by thicker crust in the neighbouring
460 Haag-Ellsworth Whitmore (30-40 km), Antarctic Peninsula (30-38 km) and Thurston Island (28-30 km) blocks.
461 We find the highest relative proportion of likely mafic lower crust to potential felsic/intermediate crust in the
462 West Antarctic Rift System, and especially in the neighbouring Ellsworth Land. By contrasting the crustal
463 structure at Thurston Island and the West Antarctic Rift System, we suggest that the boundary between the
464 two blocks lies in the vicinity of the Pine Island Rift, ~200 km north of its previously inferred position from
465 Dalziel and Elliot (1982). In addition, from high frequency receiver functions we infer that 0.1-0.8 km thick
466 low seismic velocity subglacial sediment is present beneath 10 stations within the West Antarctic Rift System,
467 Thurston Island and Ellsworth Land. Thick subglacial sediment accumulations of this type could have acted as
468 a source for the soft sediment layers identified beneath many fast flowing West Antarctic ice streams, reducing
469 basal friction.

470 **7 Acknowledgements**

471 We would like to thank both reviewers and the editor for their constructive comments on our manuscript. We
472 thank all BAS camp staff, field guides and air unit personnel for the logistical support of the UKANET seismic
473 and GNSS networks. We similarly acknowledge all academic members, field teams and camp staff associ-
474 ated with the POLENET/ANET project and thank Kenn Borek Air and the New York Air Guard for flight
475 support. CKD and JPOD are supported by the Natural Environment Research Council [grant NE/L006065/1].
476 POLENET/ANET is supported by the National Science Foundation Office of Polar Programs [grants 0632230,
477 0632239, 0652322, 0632335, 0632136, 0632209, and 0632185]. UKANET seismic instrumentation was pro-
478 vided and supported by SEIS-UK. POLENET/ANET seismic instrumentation was provided and supported
479 by the Incorporated Research Institutions for Seismology (IRIS) through the PASSCAL Instrument Center.
480 The UKANET (www.ukanet.wixsite.com/ukanet; network code 1D; https://doi.org/10.7914/SN/1D_2016) data
481 will be accessible through the IRIS Data Management Center (<http://www.iris.edu/mda>) from January 2021.
482 POLENET/ANET (network code YT), seismic data can be accessed through the IRIS DMC. The facilities of
483 the IRIS Consortium are supported by the NSF under cooperative agreement EAR1063471, the NSF Office of
484 Polar Programs, and the DOE National Nuclear Security Administration. We would also like to thank Joe Cann
485 for helpful comments on the paper. Figures were created using the Generic Mapping Tools (GMT) software
486 (Wessel and Smith, 1998).

487 **References**

- 488 Anandakrishnan, S., Winberry, J.P. (2004). Antarctic subglacial sedimentary layer thickness from receiver
489 function analysis. *Global And Planetary Change*, **42**, pp. 167–176.
- 490 Anthony, R.E., Aster, R.C., Wiens, D., Anandakrishnan, S., Huerta, A., Winberry, J.P., Wilson, T., Rowe, C.,
491 Nyblade, A., Anandakrishnan, S., Huerta, A., Winberry, J.P., Wilson, T., Rowe, C. (2015). The Seismic
492 Noise Environment of Antarctica. *Seismological Research Letters*, **86**(1), pp. 89–100.
493 **URL:** <http://srl.geoscienceworld.org/content/86/1/89.short>
- 494 Bao, X., Sun, X., Xu, M., Eaton, D.W., Song, X., Wang, L., Ding, Z., Mi, N., Li, H., Yu, D., et al. (2015). Two
495 crustal low-velocity channels beneath SE Tibet revealed by joint inversion of Rayleigh wave dispersion and
496 receiver functions. *Earth and Planetary Science Letters*, **415**, pp. 16–24.
- 497 Baranov, a., Morelli, a. (2013). The Moho depth map of the Antarctica region. *Tectonophysics*, **609**, pp.
498 299–313.
- 499 Barletta, V.R., Bevis, M., Smith, B.E., Wilson, T., Brown, A., Bordoni, A., Willis, M., Khan, S.A., Rovira-
500 Navarro, M., Dalziel, I., et al. (2018). Observed rapid bedrock uplift in Amundsen Sea Embayment promotes
501 ice-sheet stability. *Science*, **360**(6395), pp. 1335–1339.
- 502 Behrendt, J.C. (1999). Crustal and lithospheric structure of the west Antarctic Rift System from geophysical
503 investigations - A review. *Global and Planetary Change*, **23**(1-4), pp. 25–44.
- 504 Behrendt, J.C., Cooper, A. (1991). Evidence of rapid Cenozoic uplift of the shoulder escarpment of the Ceno-
505 zoic West Antarctic rift system and a speculation on possible climate forcing. *Geology*, **19**(4), pp. 315–319.
- 506 Behrendt, J.C., LeMasurier, W.E., Cooper, a.K., Tessensohn, F., Tréhu, a., Damaske, D. (1991). Geophysical
507 studies of the West Antarctic Rift System. *Tectonics*, **10**(6), p. 1257.
- 508 Bingham, R.G., Ferraccioli, F., King, E.C., Larter, R.D., Pritchard, H.D., Smith, A.M., Vaughan, D.G. (2012).
509 Inland thinning of West Antarctic Ice Sheet steered along subglacial rifts. *Nature*, **487**(7408), p. 468.
- 510 Birkenmajer, K., Delitala, M., Narebski, W., Nicoletti, M., Petrucciani, C. (1986). Geochronology of Tertiary
511 island-arc volcanics and glacial deposits, King George Island, South Shetland Islands (West Antarctica).
512 *Bulletin of the Polish Academy of Sciences. Earth sciences*, **34**(3), pp. 257–273.
- 513 Blankenship, D., Morse, D., Finn, C., Bell, R., Peters, M., Kempf, S., Hodge, S., Studinger, M., Behrendt,
514 J.C., Brozena, J. (2001). Geologic controls on the initiation of rapid basal motion for West Antarctic ice

- 515 streams: A geophysical perspective including new airborne radar sounding and laser altimetry results. *The*
516 *West Antarctic ice sheet: behavior and environment*, **77**, pp. 105–121.
- 517 Block, A.E., Bell, R.E., Studinger, M. (2009). Antarctic crustal thickness from satellite gravity: Implications
518 for the Transantarctic and Gamburtsev Subglacial Mountains. *Earth and Planetary Science Letters*, **288**(1-
519 2), pp. 194–203.
520 **URL:** <http://dx.doi.org/10.1016/j.epsl.2009.09.022>
- 521 Brisbourne, A.M., Smith, A.M., Vaughan, D.G., King, E.C., Davies, D., Bingham, R., Smith, E., Nias, I.,
522 Rosier, S.H. (2017). Bed conditions of Pine Island Glacier, West Antarctica. *Journal of Geophysical Re-*
523 *search: Earth Surface*, **122**(1), pp. 419–433.
- 524 Brocher, T.M. (2005). Empirical relations between elastic wavespeeds and density in the Earth’s crust. *Bulletin*
525 *of the Seismological Society of America*, **95**(6), pp. 2081–2092.
- 526 Burton-Johnson, A., Halpin, J., Whittaker, J.M., Graham, F.S., Watson, S.J. (2017). A new heat flux model for
527 the Antarctic Peninsula incorporating spatially variable upper crustal radiogenic heat production. *Geophysi-*
528 *cal Research Letters*, **44**(11), pp. 5436–5446.
- 529 Chaput, J., Aster, R.C., Huerta, A., Sun, X., Lloyd, A., Wiens, D., Nyblade, A., Anandakrishnan, S., Winberry,
530 J.P., Wilson, T. (2014). The crustal thickness of West Antarctica. *J. Geophys. Res. Solid Earth*, **119**(August
531 2013), pp. 378–395.
- 532 Christensen, N.I. (1996). Poisson’s ratio and crustal seismology. *Journal of Geophysical Research: Solid*
533 *Earth*, **101**(B2), pp. 3139–3156.
- 534 Christensen, N.I., Mooney, W.D. (1995). Seismic velocity structure and composition of the continental crust:
535 A global view. *Journal of Geophysical Research: Solid Earth*, **100**(B6), pp. 9761–9788.
- 536 Dalziel, I.W. (1992). Antarctica; a tale of two supercontinents? *Annual Review of Earth and Planetary Sciences*,
537 **20**(1), pp. 501–526.
- 538 Dalziel, I.W.D., Elliot, D.H. (1982). West Antarctica: Problem child of Gondwanaland. *Tectonics*, **1**(1), p. 3.
- 539 Damiani, T.M., Jordan, T.A., Ferraccioli, F., Young, D.A., Blankenship, D.D. (2014). Variable crustal thickness
540 beneath Thwaites Glacier revealed from airborne gravimetry, possible implications for geothermal heat flux
541 in West Antarctica. *Earth and Planetary Science Letters*, **407**, pp. 109–122.
- 542 Diehl, T.M. (2008). *Gravity analyses for the crustal structure and subglacial geology of West Antarctica,*
543 *particularly beneath Thwaites Glacier*. The University of Texas at Austin.

- 544 DiVenere, V.J., Kent, D.V., Dalziel, I. (1994). Mid-Cretaceous paleomagnetic results from Marie Byrd Land,
545 West Antarctica: A test of post-100 Ma relative motion between East and West Antarctica. *Journal of*
546 *Geophysical Research: Solid Earth*, **99**(B8), pp. 15115–15139.
- 547 Donnellan, A., Luyendyk, B.P. (2004). GPS evidence for a coherent Antarctic plate and for postglacial rebound
548 in Marie Byrd Land. *Global and Planetary Change*, **42**(1), pp. 305–311.
- 549 Durrheim, R.J., Mooney, W.D. (1991). Archean and Proterozoic crustal evolution: Evidence from crustal
550 seismology. *Geology*, **19**(6), pp. 606–609.
- 551 Eagles, G., Larter, R.D., Gohl, K., Vaughan, a.P.M. (2009). West Antarctic Rift System in the Antarctic
552 Peninsula. *Geophysical Research Letters*, **36**(November), pp. 4–7.
- 553 Emry, E.L., Nyblade, a.a., Julia, J., Anandakrishanan, S., Aster, R.C., Wiens, D.a., Huerta, a.D., Wilson, T.J.
554 (2015). The mantle transition zone beneath West Antarctica: Seismic evidence for hydration and thermal
555 upwellings. *Geochemistry, Geophysics, Geosystems*, **16**(1), pp. 40–58.
- 556 Fitzgerald, P. (2002). Tectonics and landscape evolution of the Antarctic plate since the breakup of Gondwana
557 , with an emphasis on the West Antarctic Rift System and the Transantarctic Mountains. *Royal Society of*
558 *New Zealand Bulletin*, **35**, pp. 453–469.
- 559 Fretwell, P., Pritchard, H.D., Vaughan, D.G., Bamber, J.L., Barrand, N.E., Bell, R., Bianchi, C., Bingham, R.G.,
560 Blankenship, D.D., Casassa, G., Catania, G., Callens, D., Conway, H., Cook, a.J., Corr, H.F.J., Damaske, D.,
561 Damm, V., Ferraccioli, F., Forsberg, R., Fujita, S., Gim, Y., Gogineni, P., Griggs, J.a., Hindmarsh, R.C.a.,
562 Holmlund, P., Holt, J.W., Jacobel, R.W., Jenkins, a., Jokat, W., Jordan, T., King, E.C., Kohler, J., Krabill, W.,
563 Riger-Kusk, M., Langlely, K.a., Leitchenkov, G., Leuschen, C., Luyendyk, B.P., Matsuoka, K., Mouginot,
564 J., Nitsche, F.O., Nogi, Y., Nost, O.a., Popov, S.V., Rignot, E., Rippin, D.M., Rivera, a., Roberts, J., Ross,
565 N., Siegert, M.J., Smith, a.M., Steinhage, D., Studinger, M., Sun, B., Tinto, B.K., Welch, B.C., Wilson, D.,
566 Young, D.a., Xiangbin, C., Zirizzotti, a. (2013). Bedmap2: Improved ice bed, surface and thickness datasets
567 for Antarctica. *Cryosphere*, **7**(1), pp. 375–393.
- 568 Gohl, K. (2012). Basement control on past ice sheet dynamics in the Amundsen Sea Embayment, West Antarc-
569 tica. *Palaeogeography, Palaeoclimatology, Palaeoecology*, **335**, pp. 35–41.
- 570 Gohl, K., Kalberg, T., Eagles, G., Dziadek, R., Kaul, N., Spiegel, C., Lindow, J. (2015). The extent of the West
571 Antarctic Rift System in the Amundsen Sea and Bellingshausen Sea sectors.
- 572 Gohl, K., Teterin, D., Eagles, G., Netzeband, G., Grobys, J., Parsieglä, N., Schlüter, P., Leinweber, V.T., Larter,
573 R.D., Uenzelmann-Neben, G., et al. (2007). Geophysical survey reveals tectonic structures in the Amundsen

574 Sea embayment, West Antarctica. *US Geological Survey Open-File Report, 2007-1047* {<http://pubs.usgs.gov/of/2007/1047/srp/srp047/>}.

575

576 Granot, R., Cande, S.C., Stock, J.M., Damaske, D. (2013). Revised Eocene-Oligocene kinematics for the West
577 Antarctic rift system. *Geophysical Research Letters*, **40**(October 2012), pp. 1–6.
578 **URL:** <http://doi.wiley.com/10.1029/2012GL054181>

579 Grunow, M., Kent, D.V., Dalziel, I.W.D. (1991). New paleomagnetic data from Thurston Island: Implications
580 for the tectonics of west Antarctica and Weddell Sea opening. *Journal of Geophysical Research*, **96**(B11), p.
581 17935.

582 Gudmundsson, G.H. (2006). Fortnightly variations in the flow velocity of Rutford Ice Stream, West Antarctica.
583 *Nature*, **444**(7122), p. 1063.

584 Harry, D.L., Anoka, J.L., Jha, S. (2018). Geodynamic models of the West Antarctic Rift System: Implications
585 for the mantle thermal state. *Geosphere*, **14**(6), pp. 2407–2429.

586 Heeszel, D.S., Wiens, D.A., Anandakrishnan, S., Aster, R.C., Dalziel, I.W., Huerta, A.D., Nyblade, A.A.,
587 Wilson, T.J., Winberry, J.P. (2016). Upper mantle structure of central and West Antarctica from array analysis
588 of Rayleigh wave phase velocities. *Journal of Geophysical Research: Solid Earth*, **121**(3), pp. 1758–1775.

589 Helffrich, G. (2006). Extended-time multitaper frequency domain cross-correlation receiver-function estima-
590 tion. *Bulletin of the Seismological Society of America*, **96**(1), pp. 344–347.

591 Holbrook, W.S., Mooney, W.D., Christensen, N.I. (1992). The seismic velocity structure of the deep continental
592 crust. *Continental lower crust*, **23**, pp. 1–43.

593 Jordan, T., Ferraccioli, F., Leat, P. (2017). New geophysical compilations link crustal block motion to Jurassic
594 extension and strike-slip faulting in the Weddell Sea Rift System of West Antarctica. *Gondwana Research*,
595 **42**, pp. 29–48.

596 Jordan, T., Ferraccioli, F., Vaughan, D., Holt, J., Corr, H., Blankenship, D., Diehl, T. (2010). Aerogravity
597 evidence for major crustal thinning under the Pine Island Glacier region (West Antarctica). *Bulletin*, **122**(5-
598 6), pp. 714–726.

599 Julia, J., Ammon, C., Herrmann, R., Correig, A.M. (2000). Joint inversion of receiver function and surface
600 wave dispersion observations. *Geophysical Journal International*, **143**(1), pp. 99–112.

601 Kalberg, T., Gohl, K., Eagles, G., Spiegel, C. (2015). Rift processes and crustal structure of the Amundsen Sea
602 Embayment, West Antarctica, from 3D potential field modelling. *Marine Geophysical Research*, **36**(4), pp.
603 263–279.

- 604 Kennett, B., Engdahl, E. (1991). Traveltimes for global earthquake location and phase identification. *Geophys-*
605 *ical Journal International*, **105**(2), pp. 429–465.
- 606 King, E.C., Woodward, J., Smith, A.M. (2007). Seismic and radar observations of subglacial bed forms beneath
607 the onset zone of Rutford Ice Stream, Antarctica. *Journal of Glaciology*, **53**(183), pp. 665–672.
- 608 Kohnen, H. (1974). the Temperature Dependence of Seismic Waves. *Journal of Glaciology*, **13**(67), pp. 144–
609 147.
- 610 Langston, C.a. (1979). Structure under Mount Rainier, Washington, inferred from teleseismic body waves.
611 *Journal of Geophysical Research*, **84**(B9), p. 4749.
- 612 Lebedev, S., Boonen, J., Trampert, J. (2009). Seismic structure of Precambrian lithosphere: new constraints
613 from broad-band surface-wave dispersion. *Lithos*, **109**(1-2), pp. 96–111.
- 614 Lloyd, A.J., Wiens, D.a., Nyblade, A.a., Anandakrishnan, S., Aster, R.C., Huerta, A.D., Wilson, T.J., Dalziel,
615 I.W., Shore, P.J., Zhao, D. (2015). A seismic transect across West Antarctica: Evidence for mantle thermal
616 anomalies beneath the Bentley Subglacial Trench and the Marie Byrd Land Dome. *Journal of Geophysical*
617 *Research: Solid Earth*, **1**, pp. n/a–n/a.
618 **URL:** <http://doi.wiley.com/10.1002/2015JB012455>
- 619 Llubes, M., Florsch, N., Legresy, B., Lemoine, J.M., Loyer, S., Crossley, D., Rémy, F. (2003). Crustal thickness
620 in Antarctica from CHAMP gravimetry. *Earth and Planetary Science Letters*, **212**(1-2), pp. 103–117.
- 621 Lodge, A., Helffrich, G. (2009). Grid search inversion of teleseismic receiver functions. *Geophysical Journal*
622 *International*, **178**(1), pp. 513–523.
- 623 Luyendyk, B.P. (1995). Hypothesis for Cretaceous rifting of east Gondwana caused by subducted slab capture.
624 *Geology*, **23**(4), pp. 373–376.
- 625 MacAyeal, D.R., Bindschadler, R.A., Scambos, T.A. (1995). Basal friction of ice stream E, West Antarctica.
626 *Journal of Glaciology*, **41**(138), pp. 247–262.
- 627 Machado, A., Chemale, F., Conceição, R.V., Kawaskita, K., Morata, D., Oteíza, O., Van Schmus, W.R. (2005).
628 Modeling of subduction components in the Genesis of the Meso-Cenozoic igneous rocks from the South
629 Shetland Arc, Antarctica. *Lithos*, **82**(3), pp. 435–453.
- 630 Millar, I., Pankhurst, R. (1987). Rb-Sr geochronology of the region between the Antarctic Peninsula and the
631 Transantarctic Mountains: Haag Nunataks and Mesozoic granitoids. *Gondwana six: structure, tectonics,*
632 *and geophysics*, **40**, pp. 151–160.

- 633 Muto, A., Anandakrishnan, S., Alley, R.B., Horgan, H.J., Parizek, B.R., Koellner, S., Christianson, K.,
634 Holschuh, N. (2019). Relating bed character and subglacial morphology using seismic data from Thwaites
635 Glacier, West Antarctica. *Earth and Planetary Science Letters*, **507**, pp. 199–206.
- 636 Muto, A., Peters, L.E., Gohl, K., Sasgen, I., Alley, R.B., Anandakrishnan, S., Riverman, K.L. (2016). Sub-
637 glacial bathymetry and sediment distribution beneath Pine Island Glacier ice shelf modeled using aerogravity
638 and in situ geophysical data: New results. *Earth and Planetary Science Letters*, **433**, pp. 63–75.
- 639 O’Donnell, J., Brisbourne, A., Stuart, G., Dunham, C., Yang, Y., Nield, G., Whitehouse, P., Nyblade, A., Wiens,
640 D., Anadakrishnan, S., et al. (2019a). Mapping crustal shear wave velocity structure and radial anisotropy
641 beneath West Antarctica using seismic ambient noise. *Geochemistry, Geophysics, Geosystems*.
- 642 O’Donnell, J., Stuart, G., Brisbourne, A., Selway, K., Yang, Y., Nield, G., Whitehouse, P., Nyblade, A., Wiens,
643 D., Aster, R., et al. (2019b). The uppermost mantle seismic velocity structure of West Antarctica from
644 Rayleigh wave tomography: Insights into tectonic structure and geothermal heat flow. *Earth and Planetary
645 Science Letters*, **522**, pp. 219–233.
- 646 O’Donnell, J.P., Nyblade, a.a. (2014). Antarctica’s hypsometry and crustal thickness: Implications for the
647 origin of anomalous topography in East Antarctica. *Earth and Planetary Science Letters*, **388**, pp. 143–155.
- 648 Piana Agostinetti, N., Malinverno, A. (2018). Assessing uncertainties in high-resolution, multifrequency
649 receiver-function inversion: A comparison with borehole data. *Geophysics*, **83**(3), pp. KS11–KS22.
- 650 Pourpoint, M., Wiens, D., Shen, W., Aster, R.C., Nyblade, A., Wilson, T.J. (2019). Constraints on shallow
651 subglacial structure beneath Thwaites Glacier from joint inversion of receiver function and surface wave
652 data. *AGUFM*, **2019**, pp. NS11B–0632.
- 653 Ramirez, C., Nyblade, A., Emry, E., Julià, J., Sun, X., Anandakrishnan, S., Wiens, D., Aster, R., Huerta, A.,
654 Winberry, P., et al. (2017). Crustal structure of the Transantarctic Mountains, Ellsworth Mountains and Marie
655 Byrd Land, Antarctica: constraints on shear wave velocities, Poisson’s ratios and Moho depths. *Geophysical
656 Journal International*, **211**(3), pp. 1328–1340.
- 657 Ramirez, C., Nyblade, A., Hansen, S., Wiens, D., Anandakrishnan, S., Aster, R., Huerta, A., Shore, P., Wilson,
658 T. (2016). Crustal and upper-mantle structure beneath ice-covered regions in Antarctica from S-wave receiver
659 functions and implications for heat flow. *Geophysical Journal International*, **204**(3), pp. 1636–1648.
- 660 Randall, D.E., Mac Niocail, C. (2004). Cambrian palaeomagnetic data confirm a Natal Embayment location
661 for the Ellsworth—Whitmore Mountains, Antarctica, in Gondwana reconstructions. *Geophysical Journal
662 International*, **157**(1), pp. 105–116.

- 663 Reading, A.M. (2007). The seismicity of the Antarctic plate. *Special Papers-Geological Society of America*,
664 **425**, p. 285.
- 665 Rignot, E., Mouginot, J., Scheuchl, B. (2011). Ice flow of the Antarctic ice sheet. *Science*, **333**(6048), pp.
666 1427–1430.
- 667 Rudnick, R.L., Fountain, D.M. (1995). Nature and composition of the continental crust: a lower crustal per-
668 spective. *Reviews of geophysics*, **33**(3), pp. 267–309.
- 669 Schopf, J.M. (1969). Ellsworth Mountains: Position in West Antarctica due to Sea-Floor Spreading. *Science*,
670 **164**(3875), pp. 63–66.
- 671 Shen, W., Wiens, D.A., Anandakrishnan, S., Aster, R.C., Gerstoft, P., Bromirski, P.D., Hansen, S.E., Dalziel,
672 I.W., Heeszel, D.S., Huerta, A.D., et al. (2018). The crust and upper mantle structure of central and West
673 Antarctica from Bayesian inversion of Rayleigh wave and receiver functions. *Journal of Geophysical Re-*
674 *search: Solid Earth*.
- 675 Siddoway, C.S., Baldwin, S.L., Fitzgerald, P.G., Fanning, C.M., Luyendyk, B.P. (2004). Ross sea mylonites
676 and the timing of intracontinental extension within the West Antarctic rift system. *Geology*, **32**, pp. 57–60.
- 677 Smith, A.M., Murray, T. (2009). Bedform topography and basal conditions beneath a fast-flowing West Antarc-
678 tic ice stream. *Quaternary Science Reviews*, **28**(7-8), pp. 584–596.
- 679 Storey, B., Dalziel, I. (1987). Outline of the structural and tectonic history of the Ellsworth Mountains-Thiel
680 Mountains ridge, West Antarctica. *Gondwana six: structure, tectonics, and geophysics*, **40**, pp. 117–128.
- 681 Thybo, H., Artemieva, I.M. (2013). Moho and magmatic underplating in continental lithosphere. *Tectono-*
682 *physics*, **609**, pp. 605–619.
- 683 Vaughan, D.G., Smith, A.M., Nath, P.C., Le Meur, E. (2003). Acoustic impedance and basal shear stress
684 beneath four Antarctic ice streams. *Annals of Glaciology*, **36**, pp. 225–232.
- 685 von Frese, R.R.B., Tan, L., Woo Kim, J., Bentley, C.R. (1999). Antarctic crustal modeling from the spectral
686 correlation of free-air gravity anomalies with the terrain. *J. Geophys. Res.*, **104**(B11), pp. 25275–25296.
687 **URL:** <http://dx.doi.org/10.1029/1999JB900232>
- 688 Wessel, P., Smith, W.H. (1998). New, improved version of Generic Mapping Tools released. *Eos, Transactions*
689 *American Geophysical Union*, **79**(47), pp. 579–579.

- 690 Wilson, D.S., Luyendyk, B.P. (2006). Bedrock platforms within the Ross Embayment, West Antarctica: Hy-
691 potheses for ice sheet history, wave erosion, Cenozoic extension, and thermal subsidence. *Geochemistry,*
692 *Geophysics, Geosystems*, **7**(12).
- 693 Winberry, J.P., Anandakrishnan, S. (2004). Crustal structure of the West Antarctic rift system and Marie Byrd
694 Land hotspot. *Geology*, **32**(11), pp. 977–980.
- 695 Zandt, G., Myers, S.C., Wallace, T.C. (1995). Crust and mantle structure across the Basin and Range-Colorado
696 Plateau boundary at 37 N latitude and implications for Cenozoic extensional mechanism. *Journal of Geo-*
697 *physical Research: Solid Earth*, **100**(B6), pp. 10529–10548.

Table 1: Crustal thickness estimates from present and previous studies.

Crustal Block	Crustal thickness range (km)		Reference
	This study	Other studies	
West Antarctic Rift System	18-28	21-31	Winberry & Anandakrishnan (2004)
		20-25	Jordan et al. (2010)
		20-28	Baranov & Morelli (2013) and references therein
		25-28	O'Donnell & Nyblade (2014)
		21-28	Chaput et al. (2014)
		19-29	Ramirez et al. (2016)
		20-30	Shen et al. (2018)
Thurston Island	28-30	24-26	Jordan et al. (2010)
		24-28	Baranov & Morelli (2013) and references therein
		~25	O'Donnell & Nyblade (2014)
		28-35	Shen et al. (2018)
Haag-Ellsworth Whitmore	30-40	30-40	Baranov & Morelli (2013) and references therein
		28-36	O'Donnell & Nyblade (2014)
		30-37	Chaput et al. (2014)
		35-38	Ramirez et al. (2017)
		30-43	Shen et al. (2018)
Antarctic Peninsula	30-38	34-44	Baranov & Morelli (2013) and references therein
		29-34	O'Donnell & Nyblade (2014)

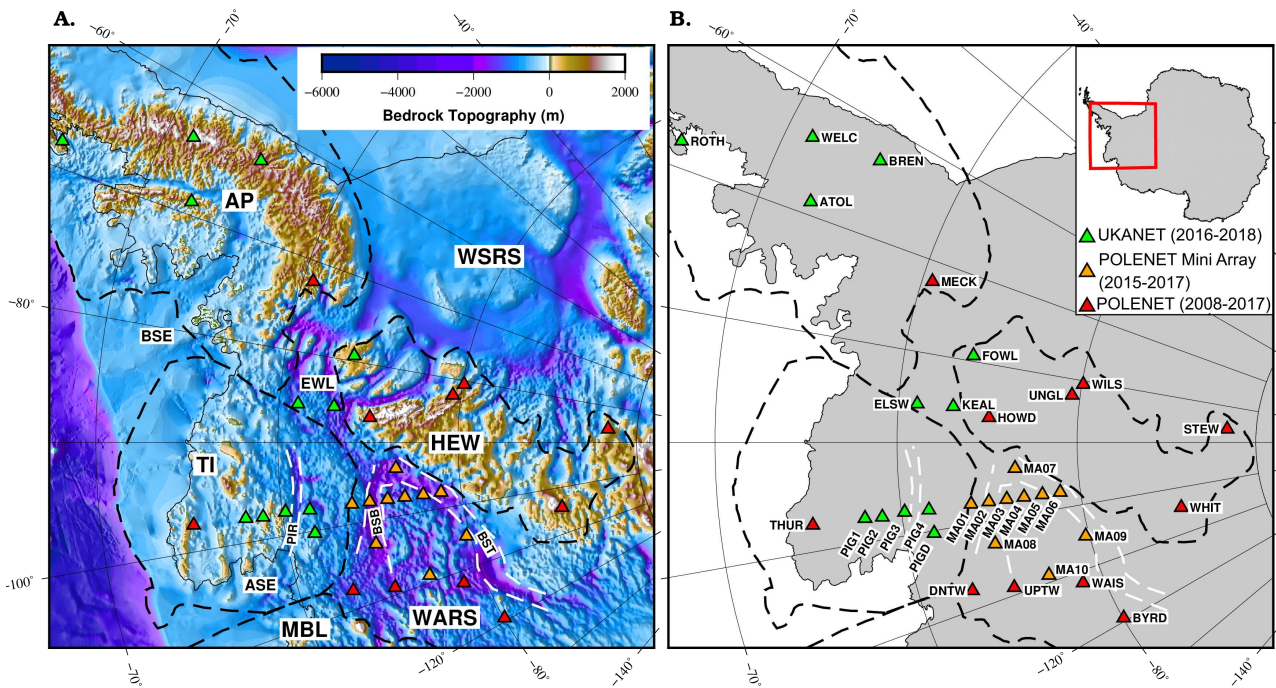


Figure 1: Maps of our study area in West Antarctica. A) BEDMAP2 bedrock topography (Fretwell et al., 2013) with the crustal block boundaries of Dalziel and Elliot (1982) displayed with black dashed lines. The crustal blocks are as follows: Antarctic Peninsula (AP), Thurston Island (TI), Marie Byrd Land (MBL), Haag-Ellsworth Whitmore block (HEW). Also included are West Antarctic Rift System (WARS), Weddell Sea Rift System (WSRS), Ellsworth Land (EWL), Amundsen Sea Embayment (ASE) and Bellingshausen Sea Embayment (BSE). Major regional structures shown with white dashed lines are the Byrd Subglacial Basin (BSB), Bentley Subglacial Trench (BST) and Pine Island Rift (PIR). B) A map highlighting the stations used in this study. The UKANET seismic network (2016-2018) is shown in green triangles, the POLENET/ANET Mini Array (2015-2017) in orange and POLENET/ANET longer term (2008 -) stations in red.

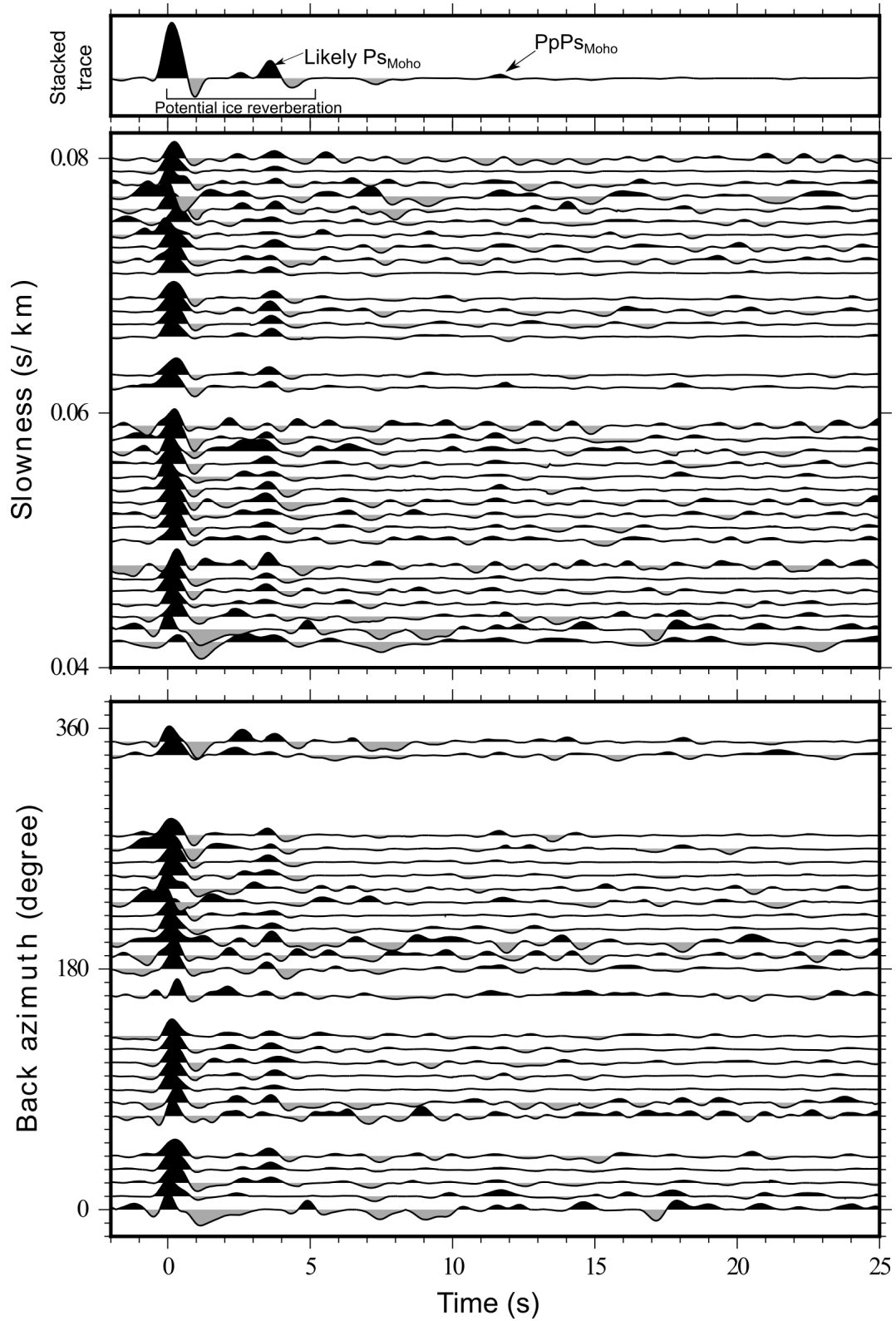


Figure 2: 2 Hz maximum frequency radial receiver functions recorded from 2016-2018 at station PIG1 (Figure 1) binned by backazimuth every 10° and slowness every 0.001 s/km. A stacked trace containing 134 individual receiver functions after quality control is displayed above. PIG1 has 1.2 km of underlying ice (Fretwell et al., 2013), as a result the relative signal contribution in the first 6 s from the crustal $P_{s_{\text{Moho}}}$ phase and ice reverberation is difficult to constrain.

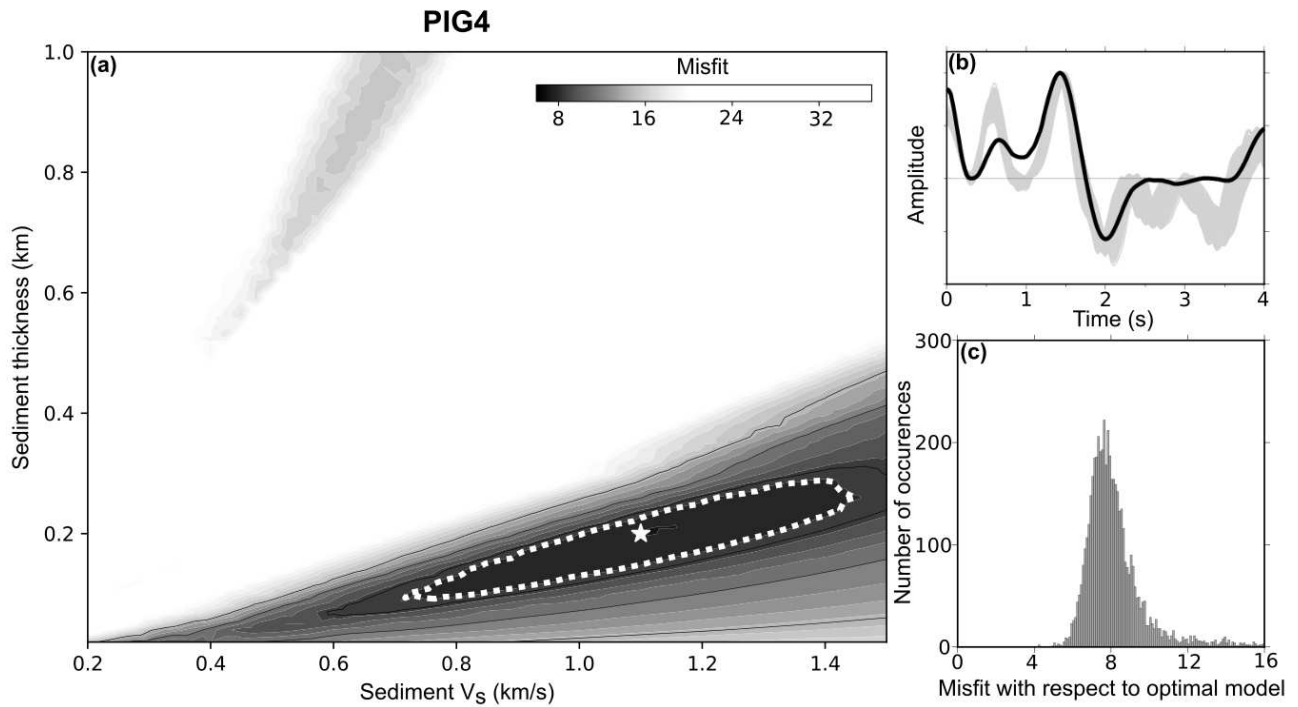


Figure 3: (a) Subglacial sediment forward modelling results for station PIG4 (Figure 1). The best fitting model is denoted by a white star, and 95% confidence bounds are shown as dashed white line. (b) Best fitting forward modelled receiver functions. The stacked receiver function is shown as a solid black line, and synthetic receiver functions from within the 95% confidence bounds are shown in grey. (c) Bootstrap analysis to estimate uncertainty of subglacial sediment forward modelling following the method of Chaput et al. (2014). We produce 5000 bootstrapped receiver functions from the data and compute misfit with respect to the best fitting models from part (a). Assuming the misfit has a normal Gaussian distribution we can then estimate 95% confidence bounds.

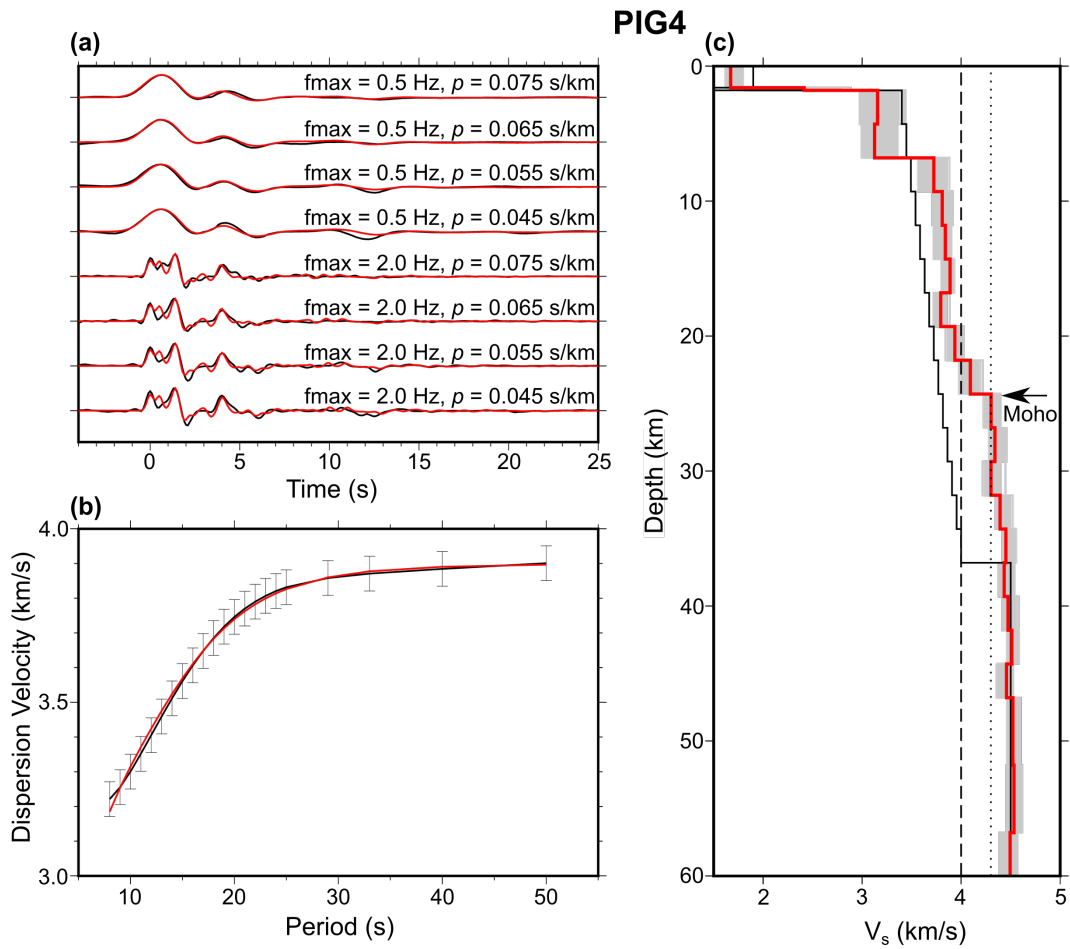


Figure 4: Joint inversion results from station FIG4. (a) Receiver functions with corresponding model results (red) stacked into narrow ray parameter (p) bins at two maximum frequencies (0.5 Hz and 2 Hz). Stacked input receiver functions are in black and the resulting inverted receiver functions are in red. (b) Rayleigh wave phase velocity dispersion curve inversion results. The input Rayleigh wave phase velocity dispersion curve is in black and the inversion result in red, showing a good fit within the ± 0.05 km/s uncertainty limits. (c) The shear wave velocity-depth profile produced by the joint inversion. The initial model is in black and the final V_s -depth profile produced by the inversion is shown in red. Models produced by 500 bootstrap iterations are displayed in grey solid lines, indicating that V_s is generally constrained to within ± 0.15 km/s. Dashed and dotted lines are added at 4.0 and 4.3 km/s respectively to indicate the layers of likely mafic lower crust.

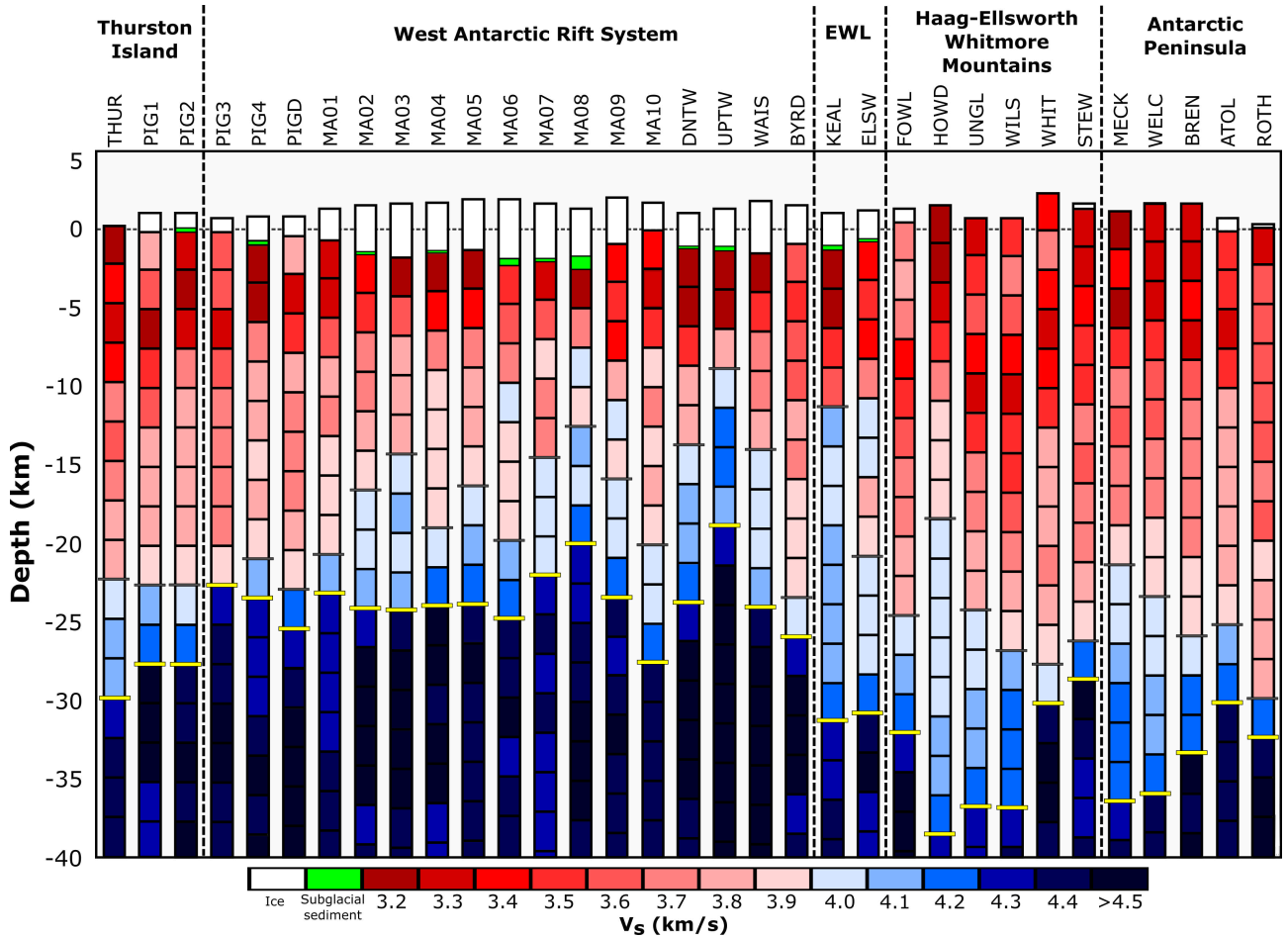


Figure 5: A summary of our V_s -depth profiles at each station, grouped by crustal block. We also group stations in the Ellsworth Land (EWL) region, given the ambiguity as to which block these stations belong. Each crustal column is coloured by modelled shear wave velocity, with red colours indicating likely felsic-to-intermediate crust and blue representing likely mafic lower crust. Upper mantle is displayed in dark blue, subglacial sediment in green, and ice in white. Our interpreted transition from felsic/intermediate crust to mafic lower crust is indicated with a horizontal grey line at each station, and our interpreted Moho with a yellow line. We include the ice thickness from Fretwell et al. (2013) and the subglacial sediment thickness identified in the forward modelling stage.

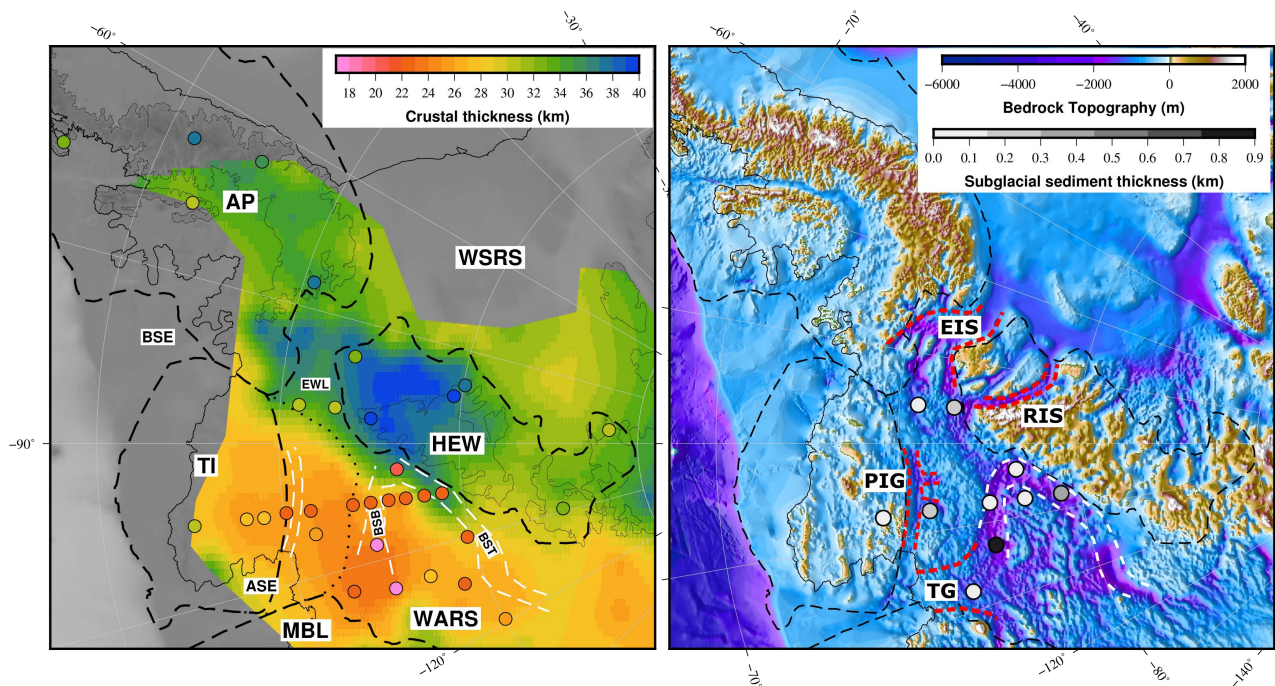


Figure 6: (Left) A map of our crustal thickness estimates at each station (circles) superimposed on the ambient noise derived crustal thickness map of O'Donnell et al. (2019a). The crustal block boundaries of Dalziel and Elliot (1982) are in dashed black except for the Thurston Island-WARS boundary which is dotted, here we have redrawn the Thurston Island-WARS boundary to encompass the thinner crust we have imaged at stations PIG3, PIG4 and MA01. (Right) A map of stations at which we infer subglacial sediment from forward modelling, coloured by layer thickness over BEDMAP2 bedrock topography. All subglacial sediment that we identify in this study lies in the WARS and Ellsworth Land, predominately at stations in the vicinity of the Byrd Subglacial Basin and Bentley Subglacial Trench. Major ice streams roughly outlined in red dashed are the following: Evans Ice Stream (EIS), Rutford Ice Stream (RIS), Pine Island Glacier (PIG) and Thwaites Glacier (TG).

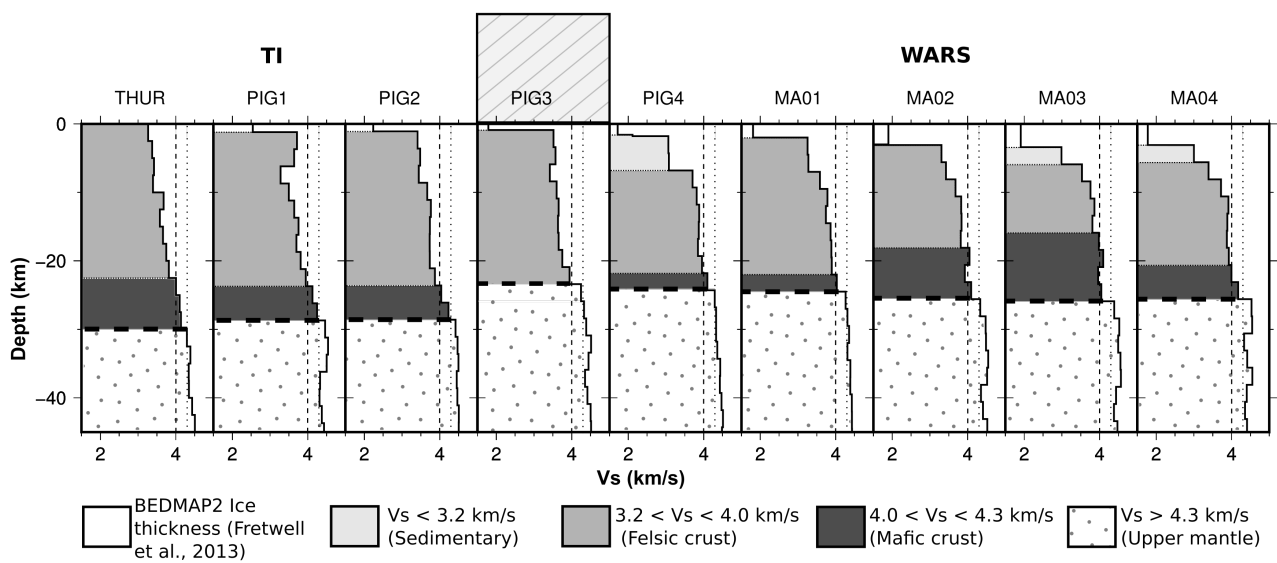


Figure 7: Shear wave velocity structure from the UKANET-POLENET/ANET Mini Array traverse stations which sample the transition from the Thurston Island (TI) block into the WARS. Our interpreted Moho is shown by a horizontal dashed black line at each station, and we add vertical dashed and dotted lines at 4.0 and 4.3 km/s respectively to indicate the transition from lower crustal to upper mantle velocities. We interpret the Thurston Island-WARS transition to lie in the vicinity of PIG3 as shown by the dashed box. Within Thurston Island we find a ~ 28 km thick crust, whilst in the WARS we find a 3 – 5 km thinner crust with a higher proportion of fast (4.0-4.3 km/s) lower crust.